Optical and Scintillation Properties of Inorganic Scintillators in High Energy Physics

Rihua Mao, *Member, IEEE*, Liyuan Zhang, *Member, IEEE*, and Ren-Yuan Zhu, *Senior Member, IEEE*

***Abstract*—This paper presents a comparative study of optical and scintillation properties for various inorganic crystal scintillators, which are used, or actively pursued, by the high energy physics community for experiments. Transmittance, excitation and photo-luminescence spectra were measured for samples with a dimension of 1.5 radiation length. The transmittance data are compared to the theoretical limit calculated by using refractive index, assuming no internal absorption. Refractive index of lutetium oxyorthosilicate and lutetium-yttrium oxyorthosilicate was measured by using a V-prism. Light output was measured for these samples with Tyvek paper wrapping, and the result is presented with the quantum efficiency of the readout devices taken out. Temperature coefficient of the light output was also measured. The result of these measurements will be used in the summary table of the inorganic scintillator section for the 2008 edition of the particle data book.**

***Index Terms*—Crystal, emission, light output, refractive index, scintillator, temperature dependence, transmittance.**

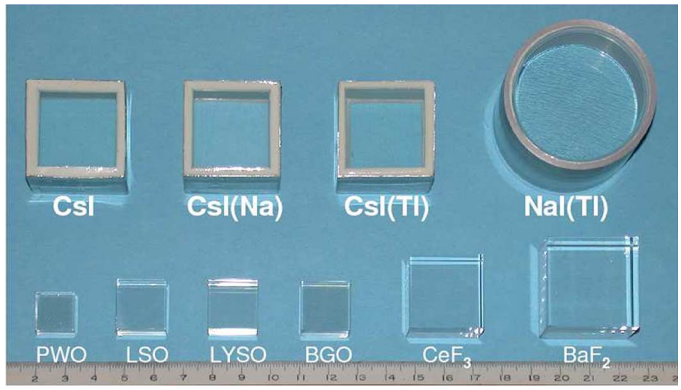

Fig. 1. A photo showing samples investigated in this work.

I. Introduction

THIS is a part of the on-going work to improve the inorganic scintillator section in the particle data book [1]. The summary table in the inorganic scintillator section of the 2006 edition includes a comparison of the light output measured by using a photomultiplier tube (PMT) with a bi-alkali cathode for various crystals with unspecified size and wrapping. Since crystal sample's light output is a product of its light yield, the light collection efficiency of the readout device and the quantum efficiency (QE) of the readout device samples of different size and wrapping material would have different light output.

To eliminate this ambiguity samples of various crystal scintillators were procured with a well defined dimension. Crystal density, or its radiation length, affects directly the detector size in high energy physics experiments since the detector depth is usually defined to fully contain electromagnetic showers of the highest energy. All samples thus are defined with a dimension of 1.5 radiation length (X_0) and the area of two end faces equaling to $1.5X_0 \times 1.5X_0$. There is no particular reason to choose 1.5, however, except that it is large enough and it is easy to maintain a full coverage with a 2" PMT.

During the light output measurement samples are wrapped with Tyvek paper, which is a standard wrapping material with good reproducibility as compared to other wrapping materials, such as Teflon films. To further facilitate a direct comparison with different readout devices, such as silicon photodiode (PD) and avalanche photodiode (APD) which are widely used in high energy physics experiments, the QE of the PMT used to measure the light output is also taken out.

In addition to the light output, optical transmittance, UV excitation and photo-luminescence spectra were also measured. A comparison of the transmittance data with its theoretical limit shows sample's optical quality. Refractive index as a function of wavelength was also measured for LSO and LYSO samples where no published data are available. Finally, the temperature dependence of the light output was also measured. The result of these measurements will be used as an input for the summary table of the inorganic scintillator section in the 2008 edition of the particle data book.

II. Samples

Fig. 1 shows all samples investigated. They are pure cesium iodide (CsI), sodium doped cesium iodide (CsI:Na), thallium doped cesium iodide (CsI:Tl), thallium doped sodium iodide (NaI:Tl) in the top row and yttrium doped lead tungstate ($PbWO_4$:Y or PWO), cerium doped lutetium oxyorthosilicate (Lu_2SiO_5: Ce, LSO) and cerium doped lutetium yttrium oxyorthosilicate ($Lu_{2(1-x)}Y_{2x}SiO_5$:Ce, LYSO), bismuth germanate ($Bi_4Ge_3O_{12}$ or BGO), cerium fluoride (CeF_3) and barium fluoride (BaF_2) in the bottom row. All these crystals have either been used in, or actively pursued for, high energy and nuclear physics experiments. It is worth to point out that recently discovered cerium doped lanthanum tri-halides, such as $LaCl_3$ and $LaBr_3$, are very bright and fast, but are not included in this study. We plan to include these samples in our further study when they are more or less in a mass-production stage.

Manuscript received January 11, 2008; revised April 24, 2008. Current version published September 19, 2008. This work was supported in part by the U.S. Department of Energy under Grant DE-FG03-92-ER-40701 and the U.S. National Science Foundation Awards PHY-0612805 and PHY-0516857.

The authors are with the California Institute of Technology, Pasadena, CA 91125 USA (e-mail: zhu@hep.caltech.edu).

Color versions of one or more of the figures in this paper are available online at http://ieeexplore.ieee.org.

Digital Object Identifier 10.1109/TNS.2008.2000776

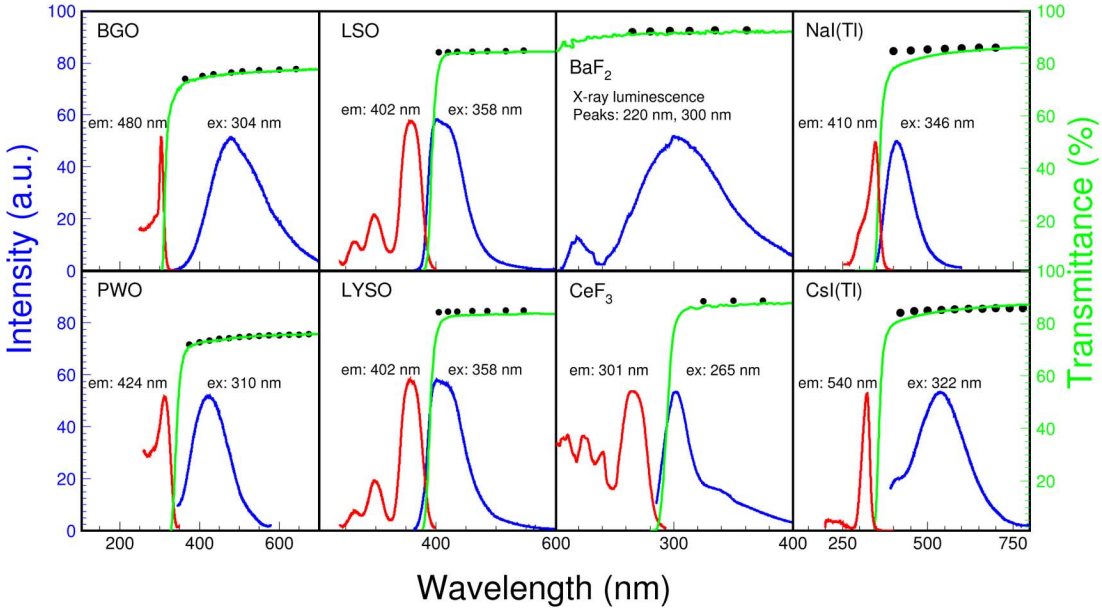

Fig. 2. Excitation (red), photo-luminescence (blue) and optical transmittance (green) are shown as a function of wavelength for heavy crystal scintillators commonly used in high energy physics experiments. The solid black dots represent the theoretical limit of the transmittance.

Samples are arranged in an order of their density, or radiation length. Crystal scintillators in the top row are hygroscopic.

The CsI and NaI based samples were procured from Institute for Scintillation Materials, Khar'kov. Because of the hygroscopicity these samples are sealed in 3 mm thick quartz windows to prevent surface damage. $PbWO_4$, BGO, CeF_3 and BaF_2 samples are provided by Shanghai Institute of Ceramics, Shanghai. LSO and LYSO samples are procured from CTI Molecular Imaging and Saint-Gobain Ceramics & Plastics, Inc. respectively. According to the manufacturers, the yttrium content is about 10% for the Saint-Gobain LYSO. The nominal cerium doping level is 0.2% for the CTI LSO and is less than 1% for the Saint-Gobain LYSO. All these samples are of mass-production quality, which may be different from samples in early development stage before the optimization is finalized. All samples, except the NaI:Tl sample, have a cubic shape with a dimension of 1.5 X_0. The NaI:Tl sample is a cylinder of 1.5 X_0 long with the area of two end faces equal to $1.5X_0 \times 1.5X_0$ to match the 2 inch PMT.

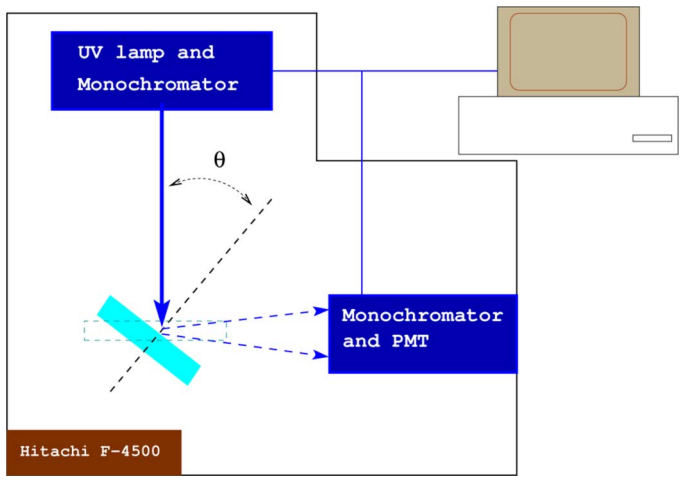

Fig. 3. The setup used for excitation and photo-luminescence measurement, where $\theta = 10^\circ$ (solid) and 0° (dashed) lead to the measured photoluminescence spectra without and with internal absorption.

III. Transmission, Excitation and Photo-Luminescence

Fig. 2 shows a comparison of the transmittance (green lines, right scale), photo-luminescence (blue lines) and excitation (red lines) spectra as a function of wavelength for eight samples. The UV excitation and photo-luminescence spectra were measured by using a Hitachi F4500 fluorescence spectrophotometer, as shown in Fig. 3. The angle θ between the excitation beam and the sample normal was set to be 10° so that the photo-luminescence spectra collected are not affected by internal absorption in the sample. As a comparison, this figure also shows a sample position with $\theta = 0^\circ$ (dashed), where measured photo-luminescence spectra would be affected by internal absorption. Internal absorption does affect the shape of the emission spectra, causing a red shift of the luminescence peak wavelength. This effect is more visible for LSO, LYSO and CeF_3 crystals since a part of their emission is self-absorbed [2]. Two emission peaks are observed for the BaF_2 sample. They are a fast component peaked at 220 nm and a slow component peaked at 300 nm.

Optical transmittance was measured by using a Perkin Elmer Lambda-950 spectrometer equipped with double beam, double monochromator and a general purpose optical bench with light path up to 40 cm. The systematic uncertainty in repeated measurements is about 0.15%. The solid black dots in Fig. 2 represent the theoretical limit of the transmittance, $T_s(\lambda)$, which is calculated according to [3] by using the refractive index data of BGO [4], BaF_2[5], NaI [6], $PbWO_4$ [7], [8], CeF_2 [9] and

TABLE I
REFRACTIVE INDEX OF LSO AND LYSO CRYSTALS

Wavelength (nm)	405	420*	436	461*	486	516*	546
Refractive index	1.833±0.001	1.827±0.001	1.822±0.001	1.818±0.001	1.813±0.001	1.810±0.001	1.806±0.001

*: Refractive index values were determined by a linear interpolation.

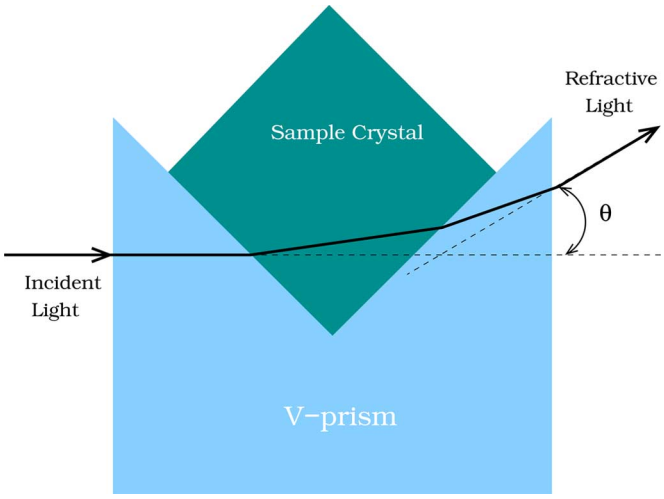

Fig. 4. The setup used to measure refractive index with a V-prism.

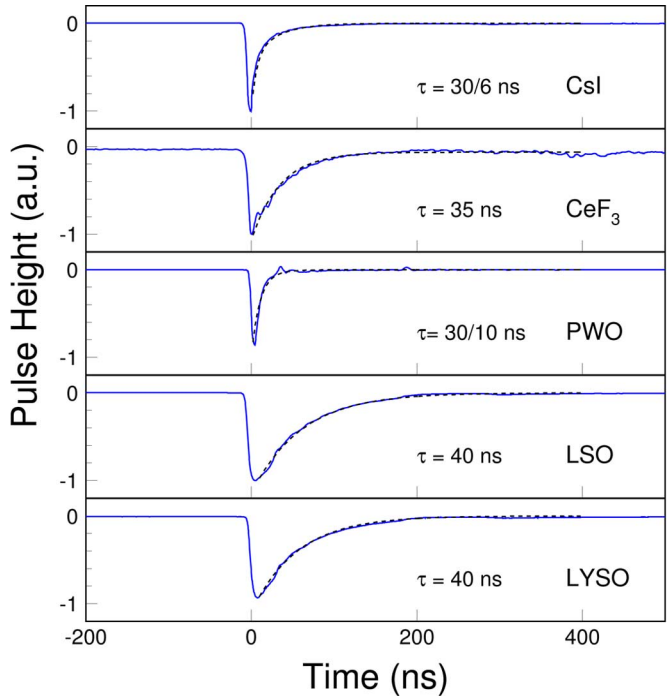

Fig. 5. Scintillation light pulse readout by a PMT and recorded by an Agilent 6052A digital scope is shown for five fast crystals with the decay time from an exponential fit (dashed lines).

CsI [10], assuming multiple bouncing between two parallel end surfaces and no internal absorption

$$T_s(\lambda) = \frac{1 - R(\lambda)}{1 + R(\lambda)}, \tag{1}$$

where

$$R(\lambda) = \frac{[n(\lambda)_{\text{crystal}} - n(\lambda)_{\text{air}}]^2}{[n(\lambda)_{\text{crystal}} + n(\lambda)_{\text{air}}]^2}. \tag{2}$$

We note that PWO crystals are birefringent. The difference of the refractive index measured along different axis is at a level of 10% as discussed in [7], [8]. Its consequence to the theoretical limit of transmittance calculated along different optical axis is discussed in details in [11].

Since there is no existing refractive index data as a function of wavelength in literature for LSO and LYSO, their refractive index between 405 and 546 nm was measured by using a V-prism, as shown in Fig. 4 [12]. The sample crystal was coupled to the V-prism with optical oil, which has a similar refractive index of the V-prism. The refractive angle between the incident light and the refractive light is a function of the refractive indices of the sample and the V-prism. By measuring the refractive angle as a function of wavelength, sample's refractive index $n(\lambda)$ can be determined as a function of the overall refractive angle $\theta(\lambda)$ and the refractive index of the V-prism $N(\lambda)$:

$$n(\lambda) = \sqrt{N(\lambda)^2 + \sin\theta(\lambda)\sqrt{N(\lambda)^2 - \sin^2\theta(\lambda)}}. \tag{3}$$

Table I shows the numerical result of the refractive index of LSO and LYSO. The result at 420 nm agrees well with that in the original patent [13]. In the wavelength region of this measurement no difference was found between the refractive indices obtained from LSO and LYSO samples.

A comparison of the measured optical transmittance and its theoretical limit T_s reveals sample's overall optical quality. As shown in Fig. 2, the measured transmittance approaches the theoretical limits for all samples, indicating very good optical quality of these samples. It is also interesting to note that while the BGO, BaF_2 and CsI(Tl) crystals have their emission spectra well within the transparent region, the UV absorption edge in the transmittance spectra of the LSO, LYSO, CeF_2, NaI(Tl) and $PbWO_4$ samples, however, cuts into the emission spectra and thus affects crystal's light output. This effect is more seriously observed in long LSO and LYSO samples as discussed in details in [14] and [15].

With recent interest of the high energy physics community in measuring both the scintillation and Cherenkov light, we also note that the values of the cut-off wavelength, at which the transmittance data show 50% of that at 800 nm, are 140 nm, 280 nm, 293 nm, 315 nm, 318 nm, 342 nm, 358 nm, 365 nm and 390 nm for BaF_2, CsI, CeF_3, BGO, CsI(Na), PWO, CsI(Tl), NaI(Tl) and LSO/LYSO respectively.

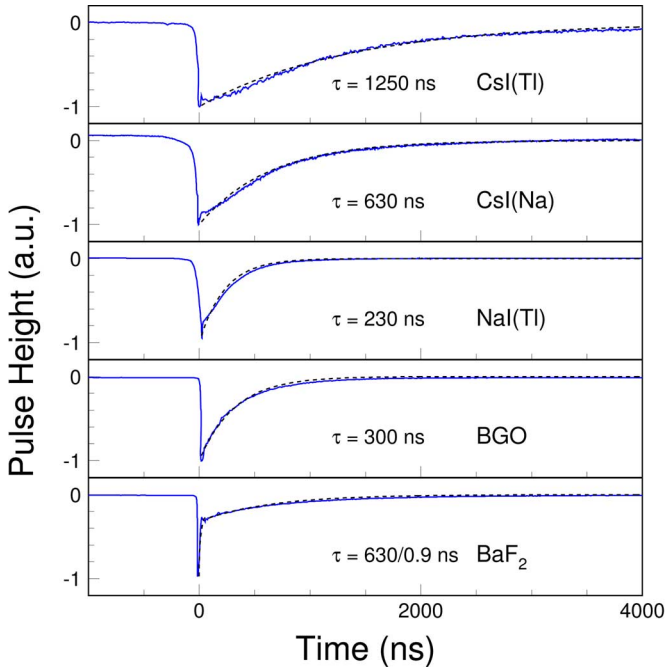

Fig. 6. Scintillation light pulse readout by a PMT and recorded by an Agilent 6052A digital scope is shown for five slow crystals with the decay time from an exponential fit (dashed lines).

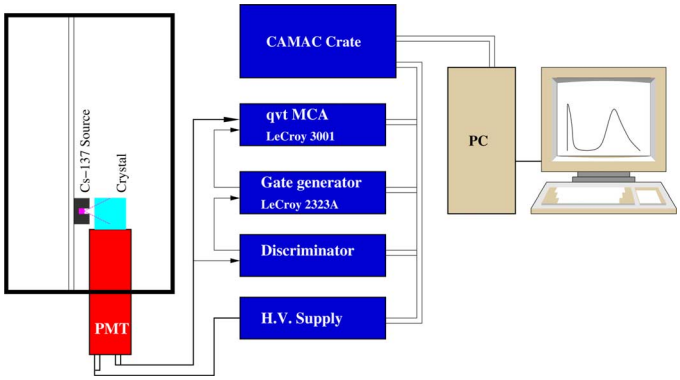

Fig. 7. The setup used for the light output measurement.

IV. Light Output and Decay Kinetics

Figs. 5 and 6 show a statistical average of 1,024 scintillation pulse shape readout by a PMT with fast response time and recorded by an Agilent 6052A digital scope for five fast and slow crystal scintillators respectively, which are excited by a ^{137}Cs source. The numerical values of their decay time listed in these figures were extracted by an exponential fit (dashed lines) to the pulse shape. The scintillation light output and decay kinetics were also measured at the room temperature (20°C) by using a Photonis XP2254b PMT, which has a multi-alkali photo cathode and a quartz window. The setup used in this measurement is shown in Fig. 7. In this measurement one end of the sample was coupled to the PMT with Dow Corning 200 fluid, while all other faces of the sample were wrapped with Tyvek paper. A collimated ^{137}Cs source was used to excite the sample. The integration time used was ranged from 45 to 4,000 ns. The

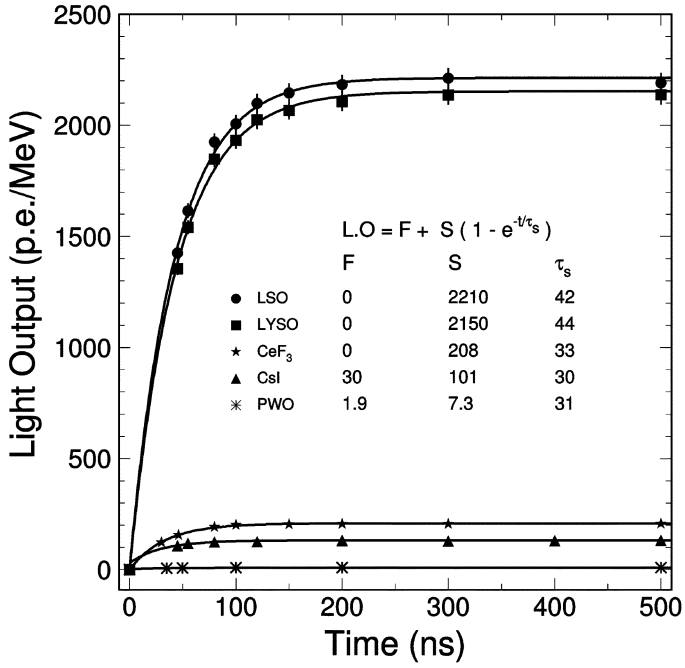

Fig. 8. Light output measured by using a Photonis XP2254b PMT is shown as a function of integration time for five fast crystal scintillators.

γ-ray peak position was determined by a simple Gaussian fit, and was used to determine sample's light output in a unit of photoelectrons per MeV energy deposition by using calibration of the single photoelectron peak.

The light output as a function of the integration time was fit to the following function to determine the fast and slow components and the decay kinetics:

$$LO(t) = F + S(1 - e^{-t/\tau_s}), \tag{4}$$

where F is the fast component of the scintillation light with a decay time of less than 10 ns, and S represents the slow component with a decay time of τ_s longer than 10 ns.

The light output shown in Figs. 8 and 9 are in unit of photoelectron/MeV which depends on the QE of the readout device used. In high energy physics applications readout devices of very different QE may be used, such as Si PD and APD. It thus is useful to take the QE of the Photonis XP2254b PMT out. The light output in unit of photon/MeV is calculated as

$$\frac{\text{photon}}{\text{MeV}} = \frac{\frac{\text{photoelectron}}{\text{MeV}}}{\overline{EWQE}}. \tag{5}$$

The $\overline{EWQE}$ is the emission weighted quantum efficiency calculated according to

$$\overline{EWQE} = \frac{\int QE(\lambda)Em(\lambda)\mathrm{d}\lambda}{\int Em(\lambda)\mathrm{d}\lambda} \tag{6}$$

where $QE(\lambda)$ and $EM(\lambda)$ are the QE and emission as a function of wavelength.

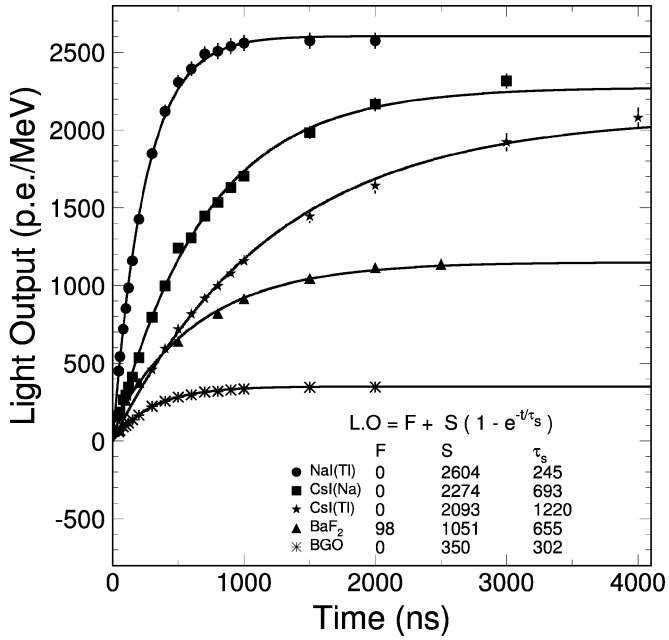

Fig. 9. Light output measured by using a Photonis XP2254b PMT is shown as a function of integration time for five slow crystal scintillators.

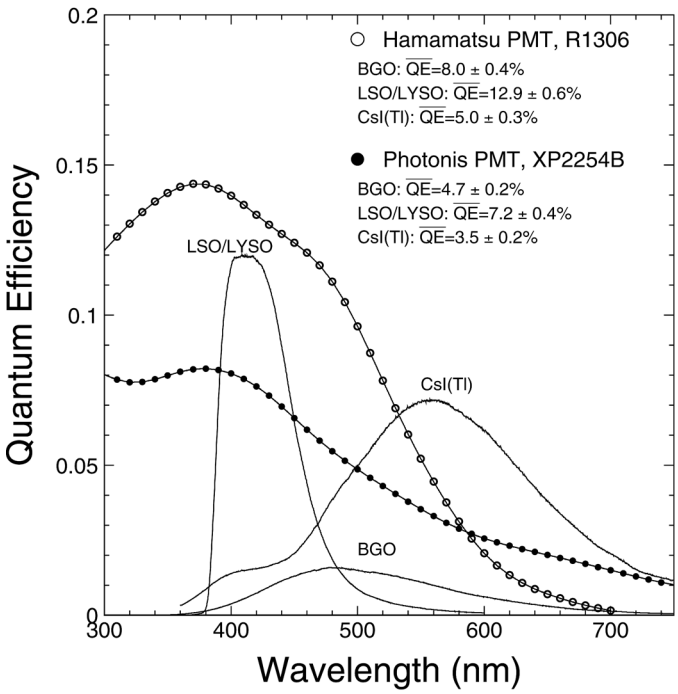

Fig. 10. The quantum efficiencies of a Hamamatsu 1306 PMT with a bi-alkali cathode (open circles) and a Photonis 2254B PMT with a multi-alkali cathode (solid dots) are shown as a function of wavelength together with the emission spectra of the LSO/LYSO, BGO and CsI(Tl) samples, where the area under the emission curves is proportional to their corresponding light output.

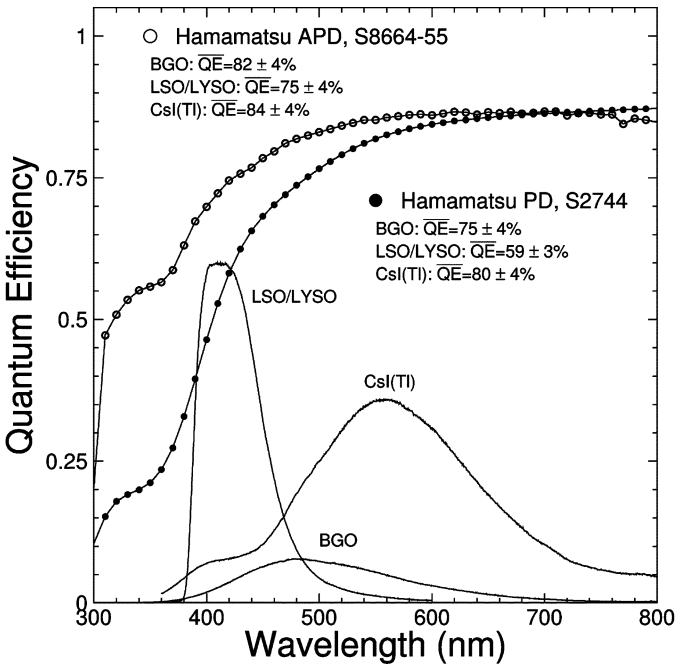

Fig. 11. The quantum efficiencies of a Hamamatsu S2744 photodiode (solid dots) and a Hamamatsu S8864-55 APD (open circles) are shown as a function of wavelength together with the emission spectra of the LSO/LYSO, BGO and CsI(Tl) samples, where the area under the emission curves is proportional to their corresponding light output.

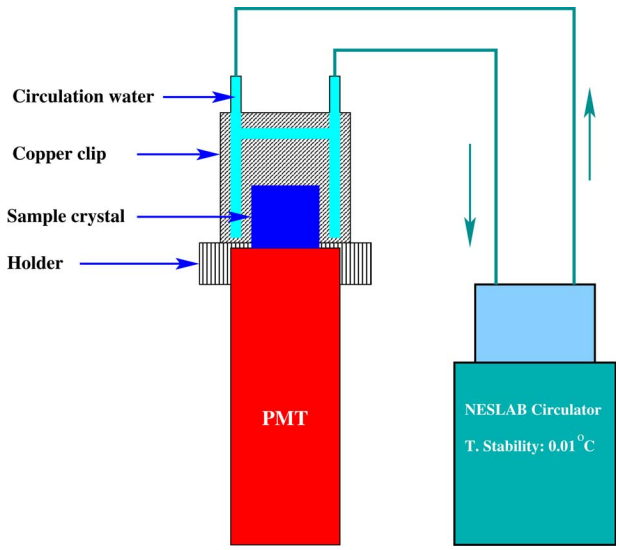

Fig. 12. The setup used for the temperature coefficient measurement.

Figs. 10 and 11 show typical QE data measured for various readout devices, such as the Photonis 2254B PMT with a multi-alkali cathode, which was used in our light output measurement (solid dots), and a Hamamatsu R1306 PMT with a bi-alkali cathode (open circles) in Fig. 10 and a Hamamatsu S2744 photodiode (solid dots) and a Hamamatsu S8864-55 APD (open circles) in Fig. 11. Also shown in these figures are the emission spectra of LSO/LYSO, BGO and CsI(Tl) crystals with the area under each emission spectrum proportional to the corresponding light output. The numerical result with QE taken out is summarized in Table II for mass-produced inorganic crystal scintillators, which have been used, or actively pursued, by the high energy and nuclear physics community for experiments. As discussed that all samples have a dimension of $1.5X_0$ and with Tyvek paper wrapping.

TABLE II
PROPERTIES OF HEAVY CRYSTAL SCINTILLATORS USED OR PURSUED BY THE HIGH ENERGY PHYSICS COMMUNITY

Crystal	NaI:Tl	CsI:Tl	CsI:Na	CsI	BaF_2	CeF_3	BGO	PWO:Y	LSO/LYSO
Density (g/cm^3)	3.67	4.51	4.51	4.51	4.89	6.16	7.13	8.3	7.40
Melting Point (°C)	651	621	621	621	1280	1460	1050	1123	2050
Radiation Length (cm)	2.59	1.86	1.86	1.86	2.03	1.70	1.12	0.89	1.14
Molière Radius (cm)	4.13	3.57	3.57	3.57	3.10	2.41	2.23	2.00	2.07
Interaction Length (cm)	42.9	39.3	39.3	39.3	30.7	23.2	22.8	20.7	20.9
Refractive Index[a]	1.85	1.79	1.84	1.95	1.50	1.62	2.15	2.20	1.82
Hygroscopicity	Yes	Slight	Yes	Slight	No	No	No	No	No
Luminescence[b] (nm)	410	550	420	420	300	340	480	425	402
(at Peak)				310	220	300		420	
Decay Time[b] (ns)	245	1220	690	30	650	30	300	30	40
				6	0.9			10	
Light Yield[b,c]	100	165	88	3.6	36	7.3	21	0.30	85
				1.1	4.1			0.077	
dLY/dT[b,d] (%/°C)	-0.2	0.4	0.4	-1.4	-1.9	~0	-0.9	-2.5	-0.2
					0.1				

a At the wavelength of the emission maximum.

b Top line: slow component, bottom line: fast component.

c Relative light output with QE of the readout device taken out for samples of 1.5 X_0.

d At room temperature (20°C).

TABLE III
TEMPERATURE COEFFICIENT OF LIGHT Yield*

Samples	NaI:Tl	CsI:Tl	CsI:Na	CsI	BaF_2	CeF_3	BGO	PWO:Y	LSO	LYSO
dLY/dT measured between 5°C and 35°C	- 0.2	0.3	0.4	- 1.3	- 1.3	-0.1	-0.9	-2.7	- 0.2	- 0.2
dLY/dT measured between 15°C and 25°C	- 0.2	0.4	0.4	- 1.4	0.1^f/-1.9^s	0.0	-0.9	-2.5	- 0.2	- 0.2

* In unit of %/°C and with systematic uncertainty of ±0.1%/°C

^{f} fast component, ^{s} slow component.

V. LIGHT OUTPUT TEMPERATURE COEFFICIENT

It is known that light yield of crystal scintillators may vary as a function of temperature. This variation has a consequence in detector design. The temperature coefficient, dLY/dT, of the light yield was measured for ten samples. Fig. 12 shows the setup used for this measurement. The temperature of the sample is controlled by a PC through a NESLAB RTE-111 cooler, which circulates water with defined temperature to a copper heat sink fixed on the sample to be measured. About 30 minutes were needed for the temperature to reach an equilibrium. Light yield was first measured as a function of temperature between 5°C and 35°C. The numerical result of the temperature coefficients at 20°C was determined by a linear fit, as listed in the top row in Table III.

As shown in Fig. 2, BaF_2 has two scintillation components with very different temperature coefficients. Two band pass filters, BPF-214 and BPF-300, were used to select fast and slow scintillation component for BaF_2. Fig. 13 shows the transmittance of these filters and the scintillation emission of BaF_2. While the filter BPF-214 selects only the fast component peaked at 220 nm, the filter BPF-300 selects only the slow component peaked at 300 nm. Fig. 14 shows light output variations measured between 15°C and 25°C, and corresponding temperature

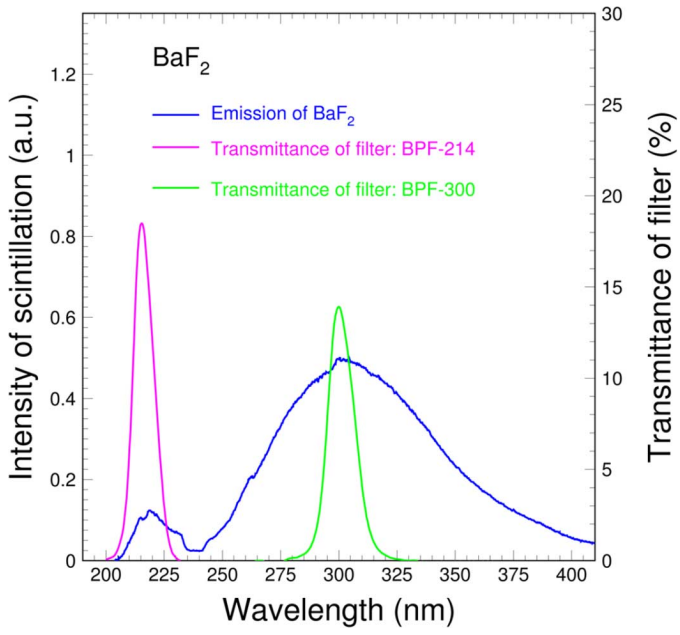

Fig. 13. The transmittance spectra of filters BPF-214 and PBF-300 and the BaF_2 emission spectrum are shown as a function of wavelength.

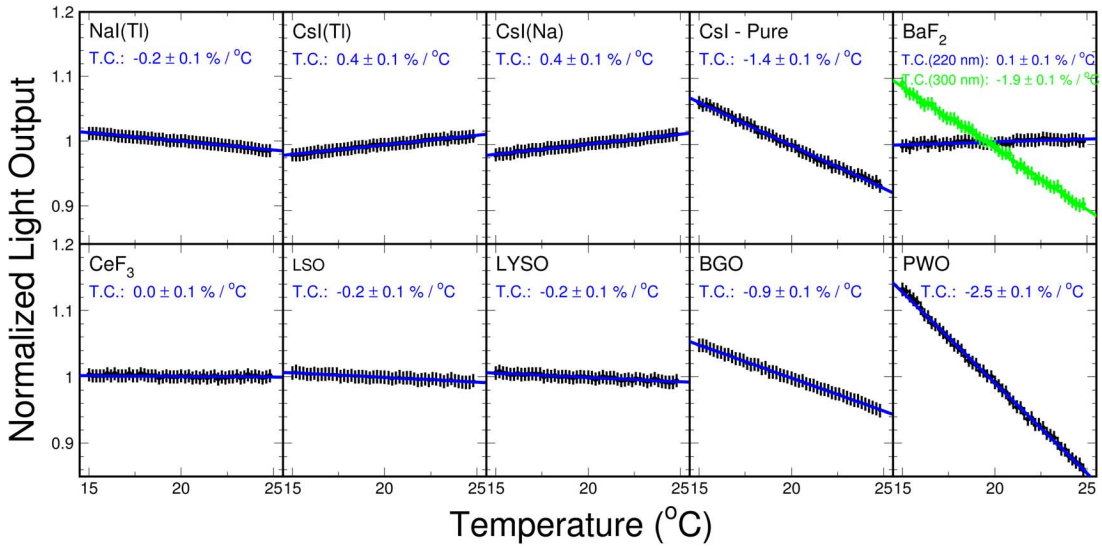

Fig. 14. Light output temperature coefficient obtained from linear fits between 15 and 25°C for commonly used crystal scintillators.

coefficients obtained by linear fits for ten samples. The numerical result of these fits is listed in the bottom row in Table III and also in Table II. As shown in Table III these two measurements are consistent.

VI. Summary

A comparative study on inorganic crystal scintillators was carried out. Refractive index as a function of wavelength were measured for LSO and LYSO by using a V-prism. Relative light output was determined for crystal samples with a dimension of $1.5X_0$ and Tyvek paper wrapping, and with quantum efficiencies of the readout devices taken out. Light output temperature coefficients at the room temperature (20°C) were also determined. Result presented here will be used in the inorganic scintillator section of the 2008 particle data book.

Acknowledgment

The authors would like to thank the Shanghai Institute of Ceramics for providing samples in this test, and Dr. G. Zhao of the Shanghai Institute of Optics and Fine Mechanics for allowing the publishing of the refractive index data he measured for the LSO and LYSO samples.

References

[1] Particle Data Group, Section 28.3, "Inorganic scintillators," *J. Phys. G: Nucl. Part. Phys. 33*, pp. 275–277, 2006.

[2] R. H. Mao, L. Y. Zhang, and R. Y. Zhu, "Emission spectra of LSO and LYSO crystals excited by UV light, x-ray and γ -ray," *IEEE Trans. Nucl. Sci.*, vol. 55, no. 3, pp. 1759–1766, Jun. 2008.

[3] D. A. Ma and R. Y. Zhu, "Light attenuation length of barium fluoride crystals," *Nucl. Instrum. Methods Phys. Res. A*, vol. A333, pp. 422–424, 1993.

[4] P. A. William *et al.*, "Optical, thermo-optic, electro-optic, and photoelastic properties of bismuth germanate," *Appl. Opt.*, vol. 35, no. 19, pp. 3562–3562, 1996.

[5] I. H. Malitson, "Refractive properties of barium fluoride," *J. Opt. Soc. Amer.*, vol. 54, no. 5, pp. 628–628, 1964.

[6] H. H. Li, "Refractive index of alkali halides and its wavelength and temperature derivatives," *J. Phys. Chem. Ref. Data*, vol. 5, no. 2, pp. 329–329, 1976.

[7] G. F. Bakhshieva and A. M. Morozov, "Refractive-indexes of molybdate and tungstate single-crystals having scheelites structure," *Sov. J. Opt. Technol.*, vol. 44, no. 9, pp. 542–542, 1977.

[8] S. Baccaro *et al.*, "Ordinary and extraordinary complex refractive index of the lead tungstate $(PbWO_4)$ crystal," *Nucl. Instr. Methods Phys. Res. A*, vol. A385, pp. 209–209, 1997.

[9] P. Chindaudom and K. Vedam, "Characterization of inhomogeneous transparent thin films on transparent substrates by spectroscopic ellipsometry: Refractive indices $n(\lambda)$ of some fluoride coating materials," *Appl. Opt.*, vol. 33, no. 13, pp. 2664–2664, 1994.

[10] W. S. Rodney, "Optical properties of cesium iodide," *J. Opt. Soc. Amer.*, vol. 45, no. 11, pp. 987–987, 1955.

[11] R. H. Mao, L. Y. Zhang, and R.-Y. Zhu, "Quality of mass-produced lead tungstate crystals," *IEEE Trans. Nucl. Sci.*, vol. 51, pp. 1777–1783, 2004.

[12] G. Zhao, private communication.

[13] C. Melcher, "Lutetium orthosilicate single crystal scintillation detector," U.S. Patent 5 025 151, 1991.

[14] J. M. Chen, L. Y. Zhang, and R.-Y. Zhu, "Large size LYSO crystals for future high energy physics experiments," *IEEE Trans. Nucl. Sci.*, vol. 52, no. 6, pp. 3133–3140, Dec. 2005.

[15] J. M. Chen, R. H. Mao, L. Y. Zhang, and R. Y. Zhu, "Large size LSO and LYSO crystal for future high energy physics experiments," *IEEE Trans. Nucl. Sci.*, vol. 54, no. 3, pp. 718–724, Jun. 2007.